UCRL- 93929
PREPRINT

SUPERCRITICAL FLUID PHASE SEPARATIONS: IMPLICATIONS FOR DETONATION PROPERTIES OF CONDENSED EXPLOSIVES

Francis H. Ree
University of California
Lawrence Livermore National Laboratory
Livermore, CA 94550

This paper was prepared for submittal to
The Journal of Chemical Physics

January 1986

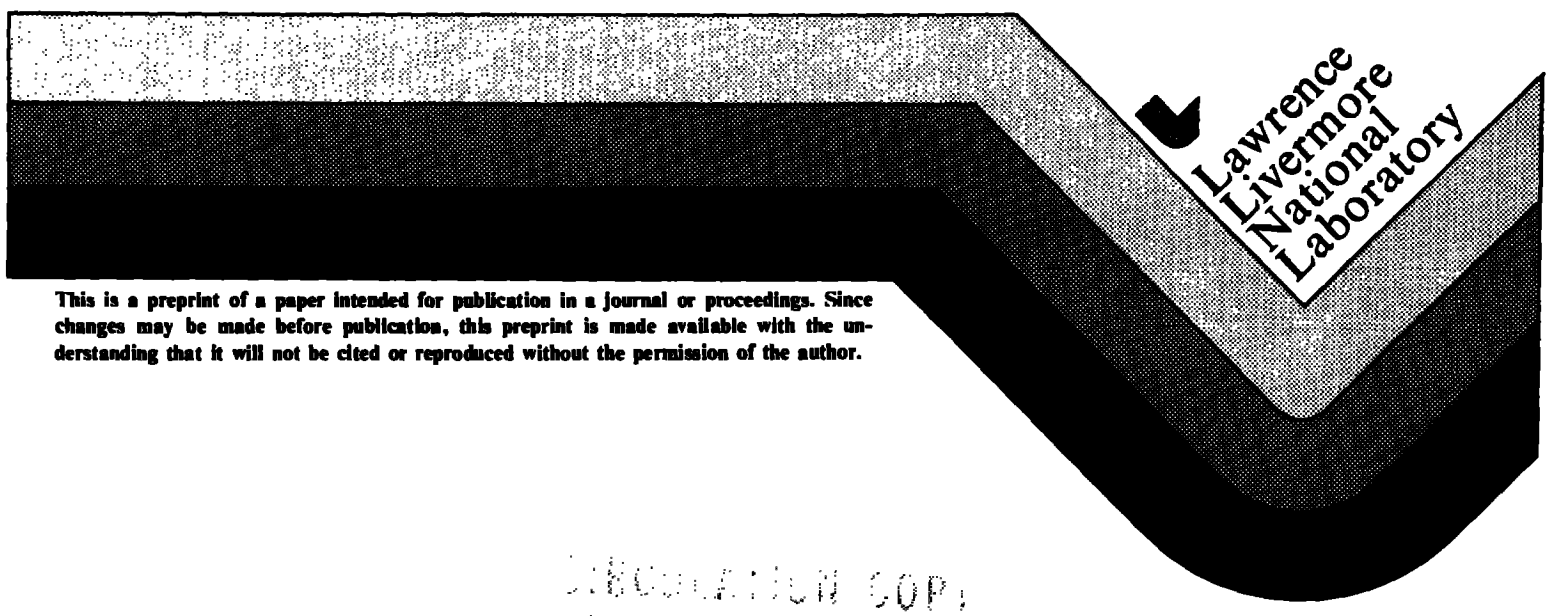

SUPERCRITICAL FLUID PHASE SEPARATIONS: IMPLICATIONS FOR DETONATION PROPERTIES OF CONDENSED EXPLOSIVES

Francis H. Ree
University of California
Lawrence Livermore National Laboratory
Livermore, CA 94550

High explosive experiments offer the most extensive data on mixtures at high pressures (> 10 GPa = 100 kbar) and high temperatures (> 1000 K). We have computed the detonation properties of two explosives, PBX-9404 ($C_{1.4}H_{2.75}N_{2.57}O_{2.67}Cl_{0.03}P_{0.01}$) and PETN ($C_4H_8N_8O_8$), using reliable statistical mechanical theories and realistic intermolecular potentials. The composition of the chemical species is determined by minimizing the Gibbs free energy. The calculation shows that the detonation products of explosives containing C, H, N, and O atoms can separate into N_2-rich and N_2-poor fluid phases and that this gas-gas phase separation can affect detonation properties at some pressures and temperatures. Since N_2, CO_2, and H_2O molecules are major detonation products, we made a separate study on binary (N_2-H_2O, CO_2-H_2O, N_2-CO_2) and ternary (N_2-CO_2-H_2O) mixtures. The results of this study show that the N_2-H_2O system may exhibit a fluid phase separation at pressures and temperatures relevant to a detonation environment. The predicted phase separation boundary is sensitive to the N_2-H_2O interaction and to the addition of CO_2 molecules. We suggest static and dynamic experiments on N_2-H_2O mixtures that should reveal whether the predicted fluid phase separation occurs and help us refine the N_2-H_2O interaction potential.

1. Introduction

The detonation of modern explosives produces a mixture of many chemical species. Typical products are N_2, CO, CO_2, H_2O, and solid carbon plus minor amounts of H_2, NH_3, O_2, NO, etc. Since explosives experiments can attain a wide range of pressures (P = 1 to 100 GPa) and temperatures (T = 1000 K to 5000 K) that are difficult to attain by static experiments on mixtures, the availability of explosives data provides us with an attractive opportunity to investigate mixtures under extreme conditions of pressure and temperature.

Fickett[1] made the first attempt in this direction in 1962, using statistical mechanics and intermolecular potentials. Recent theoretical and experimental developments have renewed interest in this field. As a result, we now have several theoretical models to describe detonation properties.[2-5]

In this regard there is the still unanswered question of whether a supercritical fluid phase separation among detonation products may influence detonation properties. Although this has not been investigated previously, the possibility is real in view of the fact that explosives experiments cover a wide (P,T) range. The present paper addresses this question.

Van der Waals first predicted a supercritical fluid phase separation in 1894.[6] The experimental confirmation of his prediction came nearly a half century later. Since Krichevskii's first experiment on a N_2-NH_3 mixture,[7] Soviet workers have found supercritical phase separations in many binary mixtures. Tsiklis's 1976 review[8] quotes more than 60 such systems. For more recent work, we refer to published papers.[8-14] Until last year, Tsiklis's work[8b] on N_2-NH_3 systems to 1.8 GPa stood out as the highest pressure experiment on fluid phase separation. However, the availability of

the diamond-anvil cell technology for mixture studies is soon expected to push the maximum pressure to a much higher value.

For example, Schouten et al.[15] very recently observed the fluid phase separation in a H_2-He mixture at pressure and temperature as high as 8 GPa and 400 K. At such high pressure and temperature, the molecular interactions are almost totally repulsive. Accumulating evidence further suggests that supercritical phase separations in some binary mixtures are "the rule rather than the exception"[10b] and that, in the case of H_2-He mixture, the phase separation will persist possibly close to the limit of stability of the molecular phase of hydrogen.[10a]

In this work we consider two explosives: PBX-9404 with its main constituent HMX (octahydro-1,3,5,7-tetranitro-1,3,5,7-tetrazocine) and PETN (pentaerythritol tetranitrate). We investigated these explosives previously[2a,5] without discussing why and how supercritical fluid phase separation can influence their detonation properties. Both explosives contain relatively small amounts of carbon. Accordingly, the rate effects in the formation of solid carbon are minimized. They are useful for studying equilibrium properties. Compared to PETN, PBX-9404 detonates at lower T and higher P; hence, its detonation behavior is more susceptible to a possible fluid phase separation. The present work will, therefore, emphasize the post-detonation behavior of PBX-9404.

Because they contain multiple components and are chemically reactive, detonation products should exhibit a complex phase behavior. To simplify our analysis, we made a separate study of phase equilibria in binary (N_2-H_2O, CO_2-H_2O, and N_2-CO_2) and ternary (N_2-H_2O-CO_2) mixtures for the three major detonation products. The temperature range of interest in this work lies well

above the critical temperature of water, the least volatile member of gaseous detonation products. In this paper, we use the terms gas and fluid synonymously since their distinction disappears above the critical point of water.

Near a phase boundary, the free energy difference between two phases is very small and is, accordingly, sensitive to uncertainties in intermolecular potentials. Therefore, we should stress at the outset that our objective is <u>not</u> precise determination of the phase boundary, an impractical task at present. Rather, our goal is to determine whether mixtures of mostly N_2, CO_2, and H_2O molecules will exhibit a supercritical fluid phase separation and what effect this phase separation will have on detonation properties. This goal can be accomplished by using realistic potentials <u>well outside</u> the phase boundaries, where a large free energy difference makes thermodynamic quantities much less sensitive to uncertainties in intermolecular potentials.

Finally, our calculations employ a reliable statistical mechanical theory of mixtures and an advanced technique to handle multiphase chemical equilibria. Some of the theoretical tools employed in this work have been discussed elsewhere.[2a] Below, we present only those aspects of our model that are pertinent to the present discussion.

2. Theoretical Formulation

The chemical formula of PETN is $C_4H_8N_8O_8$, while PBX-9404 is a composite explosive with C:H:N:O:Cl:P = 1.40:2.75:2.57:2.69:0.03:0.01.[16] The calculations reported below are insensitive to the small amounts of Cl and P atoms in PBX-9404. Unless mentioned otherwise, we delete them from the

calculations. We assume that the two explosives produce nine gaseous species (H_2, N_2, CO_2, CO, O_2, CH_4, NO, H_2O, NH_4) and a solid carbon phase, i.e., graphite or diamond. Separate approximate calculation showed that other chemical species such as H, O, C_2, C_3, etc. occur in amounts too small to affect calculated results.

The Gibbs free energy G of reacting species i (= 1,2,..,s) with molar concentrations given by a set $\{n_j\}$ is

$$G(P,T,\{n_j\}) = \sum_{i=1}^{s} n_i \mu_i(P,T,\{n_j\}), \tag{1}$$

where the μ_i's are the chemical potentials for gas and solid species.

Solid carbon is not very compressible, and its equation of state (EOS) is not as sensitive to P and T as that of the gaseous species. Nor is it a dominant species in the two explosives considered in our work.[17] Therefore, we use the Murnaghan EOS that can describe experimental data of solid carbon reliably. The exact form of the Murnaghan EOS and the resulting expression for μ_i are given in Ref. 2a.

A mixture model is needed to compute μ_i for gaseous species. The improved van der Waals one-fluid (vdWlf) model[18] is used for this purpose. The improved vdWlf model assumes that the actual pair potentials and effective one-component potential both have an exponential-6 (exp-6) form

$$\phi(r) = \epsilon \left\{\frac{6}{\alpha-6} \exp[\alpha(1-r/r^*)] - \frac{\alpha}{\alpha-6} \left(\frac{r^*}{r}\right)^6\right\}, \tag{2}$$

where ϵ and r^* are the energy- and distance-scaling parameters and α measures the stiffness of the repulsion.

The exp-6 parameters for the effective one-component potential are chosen to depend on $\{n_i\}$ in the following manner:

$$(r^*)^3 = \sum_{i,j} n_i n_j (r^*_{ij})^3 \Big/ \sum_{i,j} n_i n_j \ , \tag{3}$$

$$\epsilon (r^*)^3 = \sum_{i,j} n_i n_j \epsilon_{ij} (r^*_{ij})^3 \Big/ \sum_{i,j} n_i n_j \ , \tag{4}$$

$$\alpha\epsilon (r^*)^3 = \sum_{i,j} n_i n_j \alpha_{ij} \epsilon_{ij} (r^*_{ij})^3 \Big/ \sum_{i,j} n_i n_j \ , \tag{5}$$

where subscripts denote the interaction parameters of individual pairs (i,j), and summations are confined to each fluid phase. The reliability of the improved vdWlf model has been verified by Monte Carlo simulations.[18,19]

Our model considers molecular rotational and vibrational contribution to the free energy within the ideal-gas approximation. It employs a spherical potential for nonspherical molecules.[20,21] The assumption is accurate in fluid phase for nonpolar molecules.[22-24] It is probably good for polar molecules as well since the high temperature of detonation will enhance molecular rotation, which diminishes nonsphericity, and the accompanying high pressure and high compression will break up the orientational effect of the electrostatic interaction. For polar molecules such as water, a T-dependent spherical potential,[25] derived from an <u>ab initio</u> potential,[21] can satisfactorily describe experimental shock wave data.[26,27] Since the T-dependent potential is too complex to use in the present work, we approximate it by an exp-6 form with a T-dependent ϵ, given by

$$\epsilon = \epsilon_0 \ (1 + \lambda/T) \ , \tag{6}$$

where λ/T accounts for an effective dipole contribution. At temperatures below λ, the dipole term in ϵ dominates and $\phi(r)$, at large r, reduces to the Keesom formula,[28] i.e., $\phi(r) \approx$ constant x $(Tr^6)^{-1}$.

The exp-6 parameters for like-pair interactions may be derived from the corresponding-states scaling relations[24] or shock wave data. Table I lists numerical values of the exp-6 parameters for all gaseous species used in the present work. (For further experimental references, see Ref. 2a). Comparisons of the theoretical[2b,24] and experimental shock pressures for H_2O,[26,27] N_2,[29-31] and CO_2[31] are shown in Fig. 1. The observed good agreement here occurs for $T \leq 5000$ K, which is the upper temperature range for most explosives problems. In Fig. 1 the N_2-Hugoniot data[29b] above 35 GPa become "softer" than the extrapolation of the lower pressure data. Although the softening occurs at a relatively low pressure, the corresponding shock temperature is higher (i.e., $T \geq 7000$ K)[29c] than temperatures found in most detonation problems. The aforementioned softening may be due to thermal dissociation of molecular nitrogen to a denser monatomic nitrogen liquid.[32] Our calculations include no ionic species. In the case of the Hugoniot of water, a recent Raman scattering experiment by Holmes et al.[33a] indicates no evidence of the hydrated proton H_3O^+ ion that was previously[34] thought to be responsible for the high electrical conductivity of shocked water. Only a few percent ionization of the H_2O molecules into H^+ and OH^- ions may be responsible for the observed conductivity.[33b] Note that, in the case of detonation problems, the total pressure results from the contributions by all chemical species (beside the H_2O molecules). Therefore, the ionization correction to pressure, if any, would be very small.

Unlike-pair ($i \neq j$) exp-6 parameters are computed from the combination rules,[35]

$$r^*_{ij} = k_{ij} \, (r^*_{ii} + r^*_{jj}) \, / \, 2 \, , \tag{7}$$

$$\epsilon_{ij} = (\epsilon_{ii} \epsilon_{jj})^{1/2} , \tag{8}$$

$$\alpha_{ij} = (\alpha_{ii} \alpha_{jj})^{1/2} , \tag{9}$$

where the k_{ij} represents unity for all but the H_2O-N_2 and H_2O-CO_2 pairs. For these pairs, we consider two sets of k_{ij}:

Set 1:

$$k_{N_2\text{-}H_2O} = k_{CO_2\text{-}H_2O} = 1 ,$$

$$r^*_{N_2\text{-}H_2O} = 3.575 \text{ Å}, \; r^*_{CO_2\text{-}H_2O} = 3.615 \text{ Å}. \tag{10}$$

Set 2:

$$k_{N_2\text{-}H_2O} = 1.03, \; k_{CO_2\text{-}H_2O} = 0.965 ,$$

$$r^*_{N_2\text{-}H_2O} = 3.682 \text{ Å}, \; r^*_{CO_2\text{-}H_2O} = 3.488 \text{ Å}. \tag{11}$$

Here r^*_{ij}, ϵ_{ij}, and α_{ij} in Eqs. (7) to (11) are obtained from the like-pair interaction parameters in Table I. Unless stated otherwise, the calculations in Secs. 3 and 4 employ Eq. (10) while the results in Sec. 5 are based on Eq. (11). Our choice of Eq. (11) will be explained in Sec. 4.

To compute μ_i (= $\partial A/\partial n_i$), we use the effective one-component $\phi(r)$ [Eqs. (2) to (5)] in the Helmholtz free-energy (A) expression of the Mansoori-Canfield-Rasaiah-Stell-Ross (MCRSR) theory,[36-38]

$$A \leq A_{id} + A_{HS} + (\rho/2) \int d\underline{r}\, \phi(r) g_{HS}(r) + F \ , \qquad (12)$$

where A_{id} is the ideal-gas contribution. The MCRSR theory minimizes the right-hand side of Eq. (12) with respect to the hard-sphere diameter that appears in the hard-sphere free energy (A_{HS}), the hard-sphere radial distribution function [$g_{HS}(r)$], and a small correction factor (F).[38] The MCRSR theory shows excellent agreement with computer simulation data for a wide variety of potentials that include the exp-6 form. In this regard, several newer theories[39,40] should also give equally reliable results. The expression for μ_i derived from Eq. (12) is a complex function of $\{n_i\}$, P, and T. It is given by Eqs. (23) to (34) in Ref. 2a.

The above mathematical formulations are programmed into the chemical equilibrium (CHEQ) computer code. The CHEQ code solves for $\{n_i\}$ by minimizing[41] G and computes thermodynamic quantities by taking appropriate numerical derivatives of G, Eq. (1).

3. Detonation Properties without Consideration of Fluid Phase Separation

With the theoretical tools outlined above, we are in a position to compute detonation properties. Following earlier work,[1,3,4,42,43] we first neglect supercritical fluid phase separation and assume that detonation products are in two phases, i.e.,

Gas phase: N_2, H_2O, CO_2, CO, CH_4, NH_3, H_2, O_2, NO

Solid phase: C(d)(= diamond) or C(g)(= graphite).

The CHEQ code evaluates the specific volume (V) and internal energy (E) over a range of T and P. The resulting EOS data are then used to solve for the "Hugoniot", that is the energy conservation relation,[44]

$$E = E_o + (1/2)\ (P + P_o)\ (V_o - V), \tag{13}$$

between the equilibrium state (P,E,V) behind the detonation front and the initial state (P_o, E_o, V_o) ahead of the detonation front. The shock (i.e. detonation) velocity D is related to (P,V) by[44]

$$D = V_o\ [(P - P_o)\ /\ (V_o - V)]^{1/2}. \tag{14}$$

In Fig. 2a, we compare the resulting "two-phase" Hugoniot of PBX-9404 with the data of Kineke and West[45] and the Livermore (LLNL) group.[46] At the minimum point or Chapman-Jouguet (CJ) point in Fig. 2a, the theoretical detonation velocity D_{CJ} is 9.30 km/s, compared to the experimental value of 8.78 to 8.80 km/s.[47] The deviation of this magnitude is outside experimental uncertainties. The result was entirely unexpected because the same theoretical model gave nearly perfect agreement for PETN,[2a] i.e., D_{CJ}(CHEQ) = 8.33 km/s vs D_{CJ}(experiment) = 8.30 km/s.[46a,48] A comparison of the two-phase calculations for PBX-9404 (Table III) and PETN (Table IV in Ref. 2a) showed that the PBX-9404 has a lower CJ temperature T_{CJ} (by 619 K) but a higher CJ pressure P_{CJ} (by 6.1 GPa). Since low

temperature and high pressure generally favor a fluid phase separation, the observed deviation may be the result of a possible super-critical fluid phase separation that exists among detonation products of PBX-9404.

Before elaborating on this idea, we need to rule out other possibilities. For this purpose, we made a series of CJ calculations by changing the physical parameters of the problem while maintaining the two-phase (one gas-phase mixture plus one solid phase) constraint. Table II summarizes the results on D_{CJ}, that can be measured much more precisely (within 1%) than P_{CJ}. Calculations B and C include species (C_2H_2, C_2H_6, C_3H_8, CH_3OH) and (N_2O, NO_2, HCN), respectively, both of which were omitted in the original calculation (Calculation A). Calculation D considers the effect of the "impurity" atoms P and Cl in PBX-9404. The exp-6 parameters for these minor species (Table I) are computed from the corresponding state scaling rules.[24] Hence, they may carry larger uncertainties. These uncertainties are not important, however, because the extra species themselves are present in small amounts. The D_{CJ} values from all these calculations (B to D) agree, within 0.6%, with Calculation A. Calculations E and F examine the effects of solid carbon. Calculation E excludes solid carbon, while the standard heat of formation of diamond (15 kcal/mol)[42] used by calculation F is higher than the equilibrium value (0.453 kcal/mol). The calculations are done to simulate the amorphous, less stable nature of diamonds produced during detonation. Both calculations are even worse than Calculations A through D. Finally, Calculation G employs the r* parameters [Eq. (11)] for H_2O-N_2 and H_2O-CO_2 pairs. The result differs only a little (0.5 %) from Calculation A but is still far away from the experimental value.

4. Supercritical fluid phase separations in N_2, H_2O, and CO_2 mixtures

At the CJ points of PBX-9404 and PETN computed in Sec. 3, the mole percentages of N_2, CO_2, and H_2O are 38%, 21%, and 39% of the total gas-phase species for PBX-9404, and 19%, 39%, and 37% for PETN. The three species together represent 97% and 95% of the total gaseous products. Because these species are also the dominant species in many other explosives, we have investigated the phase behavior of binary and ternary mixtures of N_2, CO_2, and H_2O.

For a binary system its phase boundary may be directly determined by the double-tangent construction method (see below). However, since we are ultimately interested in more complex multicomponent mixtures (to which the double-tangent construction method is not applicable), our analysis below employs the CHEQ code to determine the phase boundaries of the binary and ternary mixtures. As described earlier, the CHEQ code solves for the compositions of chemical species in each fluid phase (hence, the phase boundary) so that the resulting Gibbs free energy is minimum. We will explain later that the use of the CHEQ code, although more general, is applicable to (P,T) states not too close to the critical locus of a multiphase mixture.

In Fig. 3a we show the theoretical solubility isotherms for the N_2-H_2O system at four temperatures: 0.2 eV (2321 K), 0.25 eV (2901 K), 0.3 eV (3481 K), and 0.4 eV (4642 K). Phase separation regions (i.e., mixed fluid phases) occur above each of these solubility isotherms. The (T,P) range for the N_2-H_2O system in Fig. 3a is important to detonation problems. Accordingly, a proper description of detonation behavior needs to deal with the supercritical fluid phase separation in the N_2-H_2O system. In contrast,

the fluid phase separations in the CO_2-H_2O and N_2-CO_2 systems (Figs. 3b and 3c) occur at pressures above 60 GPa for the CO_2-H_2O mixture and above 80 GPa for the CO_2-N_2 mixture. These ranges lie outside the region of interest in ordinary uses of explosives.

Before proceeding further, we should mention briefly the procedure for determining the phase separation boundaries by the CHEQ code. First, we fix T and initial values for $\{n_i\}$. Then we start our calculation at a high P, where the CHEQ code can easily find the phase boundary of two fluid phases. Finally, we determine the phase boundaries at successively lower pressures until the calculation predicts a homogeneous fluid phase. Because we use the same analytic G [Eq. (1) with μ_i from Eq. (12)] to describe different fluid phases by analytic continuation, the observed homogeneous fluid phase may be thermodynamically metastable or stable. That is, when plotted against the composition, G may show an oscillatory shape with its curvature changing from plus (+) to minus (-) to plus (+). That portion of G having the positive (convex) curvature is thermodynamically stable or metastable while the negative (nonconvex) curvature represents a thermodynamically unstable region.

It is not difficult to determine the mixed phase boundary for a binary system, where there is only one composition variable. The phase boundary is given by a pair of roots (n',n"), where G has a common ("double") tangent at fixed P and T.[19] For more complex mixtures (e.g., explosives) for which the CHEQ code is designed, the composition is multidimensional and there is no well-defined procedure. The CHEQ code uses the convexity of G to solve for $\{n_i\}$. Within or near a fluid phase boundary, this procedure can lead to a local minimum (representing a metastable homogeneous phase). We can normally avoid this situation by repeating the calculation using different

initial compositions. If none of these compositions predicts the mixed phase, we consider the (P,T) state to be in a homogeneous fluid phase. Otherwise, it is in the mixed phase region. We have used binary mixtures to test the above procedure against results from the double-tangent construction discussed earlier. The present procedure works for most cases except near the lowest portions (i.e., low P < 25 GPa) of the low-T solubility isotherms, where the free energy difference is very small and insensitive to composition. Those portions of the solubitilty isotherms, where the CHEQ code is trapped in the metastable homogeneous phase, are either omitted or indicated by dashed lines in Fig. 3.

Experimental data on the N_2-H_2O system[49] and the CO_2-H_2O system[50] are limited to pressures of 0.3 and 0.35 GPa, respectively, and to temperatures below 700 K. These data lie <u>well</u> below the temperature range (> 1300 K) where our model [Eqs. (2) and (6)] of water is applicable. Nevertheless, the experimental data show a large (T,P) region of incomplete miscibility for the N_2-H_2O system and an equally large region of complete miscibility for the CO_2-H_2O system, which is consistent with the results discussed above.

There is a semi-empirical criterion on supercritical fluid phase separation. This criterion is based on the Kreglevskii-Hildebrand solubility parameter,[8a,51]

$$\Delta = 1.5\ RT_c/V_c, \tag{15}$$

where T_c and V_c denote the critical temperature and volume. According to Kreglevskii,[51] a large difference in Δ between two species implies a small solubility between them. In the present case this rule gives

Δ(atm)= 172(N_2), 391(CO_2), and 1460(H_2O).

Hence, the N_2-H_2O mixture is the least soluble system and the N_2-CO_2 mixture is the most soluble system, which agrees with our results in Fig. 3.

A large Δ value for water suggests that water molecules are principally responsible for the fluid phase separation in the N_2-H_2O system. Physically, large values of Δ and ϵ (the well-depth parameter in Table I) reflect the high critical temperature of water, which, in turn, arises from a strong electrostatic attraction among water molecules. Without the electrostatic interaction, the Hugoniot of water resembles the dotted line in Fig. 1. The Hugoniot was computed using the exp-6 parameters, (ϵ/k,r*,α) = (135 K,3.37 Å,13.5) of the JCZ3[42] and the WCA4 model.[3b] The theoretical Hugoniot, without the electrostatic interaction, gives a lower pressure than the experimental data at pressures below 30 GPa.

The fluid phase separation boundaries in Fig. 3 are sensitive to the unlike-pair interaction parameters, Eqs. (7) to (9). Our earlier study[19] of H_2-He mixture has shown that the solubility boundaries are most sensitive to changes in $r^*_{H_2\text{-He}}$ and least sensitive to changes in $\epsilon_{H_2\text{-He}}$. In the present case, not much is known experimentally about unlike-pair interactions at the pressure and temperature of interest. Therefore, we made only a cursory study of the effect of changing r^*_{ij}. The use of a 3% larger $r^*_{N_2\text{-}H_2O}$ [Eq. (11) instead of Eq. (10)] moves the solubility isotherms to much lower P (see Fig. 4). However, such a change has little effect (less than 3%) on the thermodynamic properties of PBX-9404 in the <u>homogeneous</u> fluid region. To offset this small alteration in thermodynamic properties, we reduce $r^*_{CO_2\text{-}H_2O}$ by 3.5%

[from Eq. (10) to Eq. (11)]. Both changes together leave the EOS properties of PBX-9404 in the homogeneous fluid phase nearly the same (within 1%) as those obtained using Eq. (10).

Figure 5 shows the critical lines (loci of the minima of the solubility isotherms in Fig. 3) for the three binary systems. The solid and dotted lines represent the results with and without the parameter change discussed above. For comparison, we have superimposed the Hugoniot trajectories of PBX-9404 and PETN. The CJ points of both explosives without the parameter change [Eq. (10)] lie within the homogeneous fluid phase. With the parameter change [Eq. (11)], the CJ point of PETN remains in the homogeneous phase, but that of PBX-9404 moves inside the mixed phase range. For this reason, the D_{CJ}(CHEQ) value[2a] for PETN without the fluid phase separation showed good agreement with the experiment. Note that, since the aforementioned mixed-phase behavior of PBX-9404 is an multicomponent effect, it is not possible to show it in a plot such as Fig. 5 which describes only the binary-system results.

To find out the multicomponent, mixed-phase behavior, we have investigated the supercritical fluid phase separation in the ternary system of N_2, CO_2, and H_2O. Figure 6 shows a typical solubility diagram at 35 GPa and 0.35 eV (4062 K) that lies near the theoretical CJ point of PBX-9404. The open circle in Fig. 6 indicates the composition of N_2, CO_2, and H_2O at the CJ point. The shaded area represents the mixed fluid phase based on Eq. (10). If we use Eq. (11) in place of Eq. (10), the mixed fluid phase region (i.e., the area under dotted line in Fig. 6) is enlarged considerably. This puts the CJ point within the mixed phase range.

In summary, one can place the CJ point of PBX-9404 in either the mixed or homogeneous phase by a slight (3 to 3.5%) modification of the N_2-H_2O

interaction. In the case of the rare gases, Scoles[52] estimates uncertainties of about 1.5 and 3% for the unlike-pair interaction parameters r^*_{ij} and ϵ_{ij}, respectively. The unlike-pair interactions considered in our work have larger uncertainties. Moreover, there are 36 such pairs (or 3 x 36 = 108 exp-6 parameters) for the 9 gaseous species. Therefore, 3 to 3.5% variations in the $r^*_{N_2-H_2O}$ and $r^*_{CO_2-H_2O}$ parameters are small compared to uncertainties in the net interactions of all molecular pairs. In the analysis of explosives discussed below, we adopt the modified parameters of Eq. (11).

5. Detonation Behavior with Supercritical Fluid Phase Separation

A. Hugoniot behavior

In this calculation we allow detonation products to be in two gas phases and one solid phase, i.e.,

Gas phase A : N_2, H_2O, CO, CH_4, CO_2, NH_3, H_2, O_2, NO

Gas phase B : N_2, H_2O

Solid phase : C(d), C(g).

Gas phase B is a new phase and was not considered in Sec. 3. By considering gas phase B here, we do not mean to imply that it should occur at all temperatures and pressures. It occurs only if its presence minimizes the Gibbs free energy. Note that only N_2 and H_2O molecules appear in gas phase B. This was done on the basis of the analysis in Sec. 4 and to save computing time. Calculations are insensitive to extra species in gas phase B.

In Fig. 2b we compare the Hugoniot of PBX-9404, derived from the above three-phase CHEQ calculation, with the experimental data.[47a,47b] The present calculation gives D_{CJ}(CHEQ) = 8.81 km/s vs D_{CJ} (experiment) = 8.80 km/s. This agreement between experiment and theory extends to about 60 GPa. Table III gives a further comparison between the experimental CJ data and the two- and three-phase CHEQ calculations. If we recall our earlier unsuccessful effort to account for the failure of the two-phase D_{CJ}(CHEQ) by various physical factors (Table II), the agreement seen here is all the more remarkable. It renders strong support for the predicted supercritical fluid phase separation in the detonation products of PBX-9404.

According to the present calculation, the mole percentages of detonation products at the CJ point of PBX-9404 are:

Gas phase A: N_2(2.67%), H_2O(31.92%), CO_2(17.44%), CO(0.21%), CH_4(3×10^{-3}%), NH_3(1.47%), H_2(2×10^{-3}%), O_2(7×10^{-5}%), NO(7×10^{-3}%)

Gas phase B: N_2(28.71%), H_2O(0.21%)

Solid phase: C(d)(17.34%), C(g)(0%).

This shows that N_2 molecules thermodynamically prefer to separate (mostly in phase B) from the rest. As mentioned earlier, the conclusion is valid despite the number of species in phase B. For example, if we allow CO_2 in gas phase B, about 2% of the CO_2 in phase A shifts to gas phase B with no net change in the concentration of CO_2. The (T,V,P,E,D) values at the CJ point also remain unchanged (within 0.3%). See Table III.

In the case of PETN, the phase separation boundary crosses the Hugoniot above the CJ point at 48 to 56 GPa. As disscussed earlier, PETN has a higher CJ temperature and a lower CJ pressure than PBX-9404 does; therefore, the CJ point of PETN lies in the homogeneous fluid phase. The agreement between the theoretical Hugoniot and the experimental data of Kineke[45b] is approximately similar to that of PBX-9404 in Fig. 2b.

We note in passing that the P_{CJ}(CHEQ) value for PBX-9404 in Table III is about 10% below the experimental value. A similar difference also occurs for PETN.[2a] A part of both deviations probably originates from the same source. In Ref. 2a we attributed a part of the difference to CJ pressure experiments that might have finished too early to observe slow rate processes associated with the condensation and crystallization of carbon. Above 65 GPa in Fig. 2b, the experimental Hugoniot is slightly (< 2%) softer than the CHEQ results. The exact cause of the observed small deviation is not known at present. But it may be due to nitrogen. The shock temperatures in PBX-9404 here lie above 5100 K. We have earlier noted that the Hugoniot of nitrogen (Fig. 1) becomes soft at high temperature (> 7000 K) possibly as a result of thermal dissociation.[29b] We will defer further discussion of these complex topics. They lie outside the scope of this work on fluid phase separation.

B. Chapman-Jouguet expansion adiabat

The Hugoniot experiment discussed so far provides thermodynamic data above the CJ point. A cylinder test[53] furnishes the adiabatic expansion behavior below the CJ point. An "experimental" CJ adiabat is commonly expressed by an empirical EOS expression that can reproduce cylinder-test data

and experimental CJ data. The most widely used expression for this purpose is the Jones-Wilkins-Lee (JWL) EOS. The JWL parameters for PBX-9404 and PETN have been obtained by Lee et al.[53]

Figure 7 compares the cylinder-test result (JWL) of PBX-9404 with the CHEQ calculation and two other EOS models, i.e., the Becker-Kistiakowsky-Wilson (BKW) EOS[42,43,54] and the Jacobs-Cowperthwaite-Zwisler (JCZ3) EOS.[55] The deviations between the present result and JWL stay within 5% over the volume range 0.7 V_o to 3 V_o (V_o = initial volume = 0.5435 g/cm^3). The observed deviations lie within the experimental and the theoretical uncertainties. In comparison, the JCZ3 and the BKW models deviate from the JWL model by as much as 10 and 35%, respectively.

The CJ adiabat at $V/V_o \leq 0.86$ in Fig. 7 lies within the three-phase (N_2-rich and N_2-poor fluid phases plus a diamond-like solid) region. The adiabat crosses the N_2-phase separation boundary at $V/V_o \approx 0.86$ to 0.93. At higher expansion, it enters into the two-phase region, i.e., a homogeneous fluid phase plus a graphitic or diamond-like phase, depending on whether V/V_o is greater or less than 1.2. At $V/V_o \geq 4$, all detonation products are in a single gas phase. The various phase changes are difficult to discern in Fig. 7. They show up more clearly in the second-order quantities, such as the Grüneisen gamma, $\gamma = V(\partial P/\partial E)_V$, plotted in Fig. 8. The present calculation predicts two sharp dips in γ, one associated with the graphite-to-diamond transition and another with the N_2-phase separation.

C. Experimental suggestions

The initial density (ρ_0 = 1.84 g/cm^3) of the Hugoniot experiments discussed lies close to the theoretical maximum density of PBX-9404. Similar experiments can also be performed with porous samples. Depending on their ρ_0, porous samples can attain different CJ states that belong to the one-, two-, or three-phase region of detonation products. Although such experiments have not been done for PBX-9404, P_{CJ} and D_{CJ} data[56,57] have been published for RDX [$(CH_2N_2O_2)_3$] that has the same relative composition as HMX [$(CH_2N_2O_2)_4$]. The latter constitutes 94 wt% of PBX-9404. Since the detonation behavior of RDX and PBX-9404 is almost identical, we have computed the Hugoniot of RDX, using the experimental energy (E_0 = 277.1 J/g) of formation of RDX and the CHEQ EOS data of PBX-9404.

Figure 9 shows the theoretical Hugoniots of RDX at six different ρ_0. At ρ_0 > 1.6 g/cm^3, the CJ points lie within the three-phase region of detonation products while those at ρ_0 < 1.55 g/cm^3 belong to the two-phase region. The Hugoniots for ρ_0 = 1.55 and 1.60 g/cm^3 display double minima. The corresponding (P,T) range lies within the N_2-phase separation boundary. The double mininma signify two solutions for the CJ point. Since both solutions satisfy the CJ condition (that both the detonation velocity and accompanying rarefaction waves travel with the same velocity), both can theoretically occur. Whether it is possible to distinguish both minima experimentally is not yet known. However, the D_{CJ} corresponding to the absolute minimum (marked by solid circles in Fig. 9) should be relatively easy to measure, because it is also associated with the CJ point outside of the double-root region. Cheret[58] has also predicted

similar double minima for PETN near the carbon condensation region (between ρ_0 = 1.348 and 1.354 g/cm^3).

The D_{CJ} value corresponding to the absolute minimum is a continuous function of ρ_0, with a discontinuous slope near ρ_0 = 1.55 g/cm^3 (Fig. 10a), while the corresponding P_{CJ} shows a discontinuity at the same ρ_0 (Fig. 10b). Steinberg[56] has compiled the experimental data[57] of HMX and RDX. As Steinberg notes, the present model correctly reproduces a small change in the slope of the experimental D_{CJ} data near ρ_0 = 1.18 g/cm^3 in Fig. 10a. Our model predicts the solidification of carbon at this ρ_0. Figure 9b shows that the present model gives an equally satisfactory P_{CJ}. Scatters in the experimental data make it difficult to judge whether the predicted supercritical fluid phase separation is abrupt enough to show up in the experimental data. As discussed in Sec. 4, the boundary separating the N_2-rich and N_2-poor fluid phases (marked by dotted lines in Fig. 10) is difficult to locate precisely. Accurate experiments on D_{CJ} at different ρ_0 are desirable in this regard. Table IV shows more detailed numerical comparisons between experiment and theory.

We suggest two experiments that will help check the predicted supercritical fluid phase separation. RX-23-AB, a specially formulated explosive[42] consisting of hydrogen nitrate (70 mole %), hydrazine (5.9 mole %), and water (24.1 mole %), produces chemically stable H_2O and N_2 molecules with possibly small amounts of NO, NO_2, etc. Hugoniot experiments above 40 GPa should provide a simple test of the supercritical fluid phase separation as predicted in Sec. 4.

The second experiment is a phase separation study of the N_2-H_2O system, using a heated diamond anvil cell. As stated earlier, Schouten

et al.[15] have done such an experiment for the H_2-He system. The experiment, as conceived by Constantino,[59] would entail trapping a fully miscible mixture of N_2 and H_2O in the gasketted region of the diamond cell and then, raising the pressure along an isotherm until phase separation is observed by noting the formation of regions having different indices of refraction. Since the accessible static (T,P) range of such an experiment could reach 1500 K and 20 GPa,[60] one can check for the possible existence of a miscibility gap close to the CJ point (2200 K,17 GPa) of RX-23-AB.[2b,24] This developing technology offers a variety of interesting follow-on experiments, such as laser heating the mixture and observing the phase separation using Raman or IR absorption spectra.

6. Summary

We used the multiphase, multicomponent, statistical-mechanical CHEQ model to investigate the occurrence of supercritical phase separations in binary and ternary mixtures of N_2, CO_2, and H_2O molecules and in detonation products of PBX-9404 and PETN.

The most significant result of our analysis of binary and ternary systems is that the N_2-H_2O system may exhibit a supercritical fluid phase separation in the same (T,P) range as we encounter in explosives experiments. This prediction is consistent with the experimental N_2-H_2O phase diagram at much lower (T,P) values.[49] The factor directly responsible for the predicted phase separation is the repulsive parameter $r^*_{N_2\text{-}H_2O}$. For hard-sphere mixtures with the diameter of an unlike pair (a,b), given by

$$d_{ab} = \frac{1}{2} (d_{aa} + d_{bb}) (1 + \theta), \quad (16)$$

Melnyk and Sawford[61] made molecular dynamic simulation and other theoretical calculations. Their results indicate a fluid phase separation if $\theta > 0$. If θ is zero or small, the transition occurs in the metastable fluid range. The $\theta = 0$ case has been investigated by Lebowitz and his coworkers[62] and by Alder.[63] However, as Lebowitz and Zomick noted, for real fluids at high pressures there is no compelling reason that θ should be zero.

Probably the most significant practical result for explosives is the prediction that N_2 molecules prefer to phase-separate from the rest of the detonation products. This phase separation occurs at a pressure that lies below the CJ point for PBX-9404 and above the CJ point for PETN. By incorporating the N_2-fluid phase separation in the model, we obtain better agreement with the experimental detonation data.

It should be emphasized, however, that this study involved our limited knowledge on the intermolecular forces of unlike molecular pairs. In particular, there are no high-P and high-T data on the N_2-H_2O system. Accordingly, the (P,T) boundary of the predicted fluid phase separation is difficult to locate. Our proposed experiments should corroborate the theoretical prediction and help us refine the present model. These experiments include shock wave experiments on RX-23-AB and porous PBX-9404, and a heated diamond-anvil cell experiment on the N_2-H_2O system.

We have shown that a nonempirical approach, such as that presented here, can reliably describe the detonation properties of PBX-9404 and PETN. This conclusion will likely remain true for other explosives with C, H, N, and O atoms with a low C-to-O ratio. The observed agreement between theory and

experiment indicates that these explosives can attain a rapid equilibration after detonation.

Although our work has focused on explosives, the theory employed should be applicable to other classes of multiphase, multicomponent problems. For example, (T,P) conditions in the interiors of the giant planets are similar to those of high explosives. Except for chemically inert helium, planets and explosives share the same molecular species. However, the elemental compositions of the giant planets differ from each other and from those of explosives. Therefore, we expect that the giant planets will display an entirely different class of fluid phase separations. Stevenson[64] has prepared a list of experiments and theories, needed in the field of mixtures, to help further understanding of the physics of planetary interiors.

Acknowledgments

I would like to thank W. Hoover, E. Lee, W. Nellis, D. Steinberg, C. Tarver, and M. van Thiel for reading the manuscript and for their pertinent experimental and theoretical suggestions. This work was performed under the auspices of the U.S. Department of Energy by Lawrence Livermore National Laboratory under contract W-7405-Eng-48.

0667M/0553M

References

1. (a) W. Fickett, Los Alamos National Laboratory, Los Alamos, NM, LA-2712 (1962); (b) Phys. Fluids 6, 997 (1963).

2. (a) F. H. Ree, J. Chem. Phys. 81, 1251 (1984); (b) Proceedings of the Seventh Symposium (International) on Detonation, J. M. Short, Ed., NSWL MP 82-334 (Naval Surface Weapons Center, White Oak, MD, 1981), p. 646.

3. (a) R. Chirat and G. Pittion-Rossillon, J. Chem. Phys. 74, 4634 (1981); (b) in Ref. 2b, p. 695; (c) Combust. Flame 45, 147 (1982).

4. H. D. Jones, in Ref. 2b, p. 716.

5. (a) M. S. Shaw and J. D. Johnson, Proceedings of the Eighth Symposium (International) on Detonation, to appear; (b) R. Chirat and J. Baute, ibid; (c) G. Kerley, ibid; (d) W. B. Brown, ibid; (e) F. H. Ree and M. van Thiel, ibid.

6. J. D. van der Waals, Zittingsv. K. Akad. Wet. Amsterdam (1894), p. 133.

7. (a) I. R. Krichevskii and P. E. Bol'shakov, Zhur. Fiz. Khim. 15, 184 (1941); (b) I. R. Krichevskii and D. S. Tsiklis, Zhur. Fiz. Khim, 15, 1059 (1941).

8. (a) D. S. Tsiklis, Russ. J. Phys. Chem. 50, 825 (1976); (b) D. S. Tsiklis, Doklady Akad. Nauk. S.S.S.R. 86, 1159 (1952).

9. G. M. Schneider, in Advances in Chemical Physics, Vol. 17, I. Prigogine and S. A. Rice, Eds. (Interscience, New York, 1970), p. 1.

10. (a) W. B. Streett, Icarus 29, 176 (1976); (b) W. B. Streett, Astrophys. J. 186, 1107 (1973).

11. (a) K. S. Shing and K. E. Gubbins in Molecular-Based Study of Fluids, ACS Advances in Chemistry Series, No. 204, J. M. Haile and G. A. Mansoori, Eds. (American Chemical Society, 1983), p. 73.

12. (a) E. U. Franck, in High Pressure in Science and Technology, Part II, C. Homan, R. K. MacCrone, and E. Whalley, Eds. (North-Holland, New York, 1984), p. 95; (b) E. A. Franck, Fluid Phase Equilibria 10, 211 (1983).

13. (a) C. P. Hicks and C. L. Young, J. Chem. Soc. Faraday II 73, 597 (1977); (b) L. Hurle, F. Jones, and C. L. Young, ibid, 73, 613 (1977).

14. (a) N. J. Trappeniers, J. A. Schouten, and C. A. Ten Seldam, Chem. Phys, Lett. 5, 541 (1970); (b) J. A. Schouten, C. A. Ten Seldam, and N. J. Trappeniers, Physica 73, 556 (1974).

15. J. A. Schouten, L. C. van den Bergh, and N. J. Trappeniers, Chem. Phys. Lett. 114, 401 (1985).

16. B. M. Dobratz, "LLNL Explosives Handbook - Properties of Chemical Explosives and Explosive Simulants," Lawrence Livermore National Laboratory Report, UCRL-52997 (1981), p. 19-113 and p. 19-125.

17. However, the temperature correction must be considered for explosives with high carbon content. M. van Thiel and F. H. Ree, in The Proceedings of the Fourth Topical Conference on Shock Waves in Condensed Matter (to appear).

18. F. H. Ree, J. Chem. Phys. 78, 409 (1983).

19. F. H. Ree, J. Phys. Chem. 87, 2846 (1983).

20. (a) F. H. Ree and N. W. Winter, J. Chem. Phys. 73, 322 (1980); (b) P. J. Hay, R. T. Pack, and R. L. Martin, J. Chem. Phys. 81, 1360 (1984).

21. O. Matsuoka, E. Clementi, and M. Yoshimine, J. Chem. Phys. 64, 1351 (1976). See also references cited therein.

22. (a) J. D. Johnson, M. S. Shaw, and B. L. Holian, J. Chem. Phys. 80, 1279 (1984); (b) M. S. Shaw, J. D. Johnson, and B. L. Holian, Phys. Rev. Lett., 50, 1141 (1983); (c) J. D. Johnson and M. S. Shaw, J. Chem. Phys. (submitted).

23. (a) J. L. Lebowitz and J. K. Percus, J. Chem. Phys. 79, 443 (1983); (b) D. MacGowan, E. M. Waisman, J. L. Lebowitz, and J. K. Percus, J. Chem. Phys. 80, 2719 (1984); (c) G. O. Williams, J. L. Lebowitz, and J. K. Percus, J. Chem. Phys. 81, 2070 (1984); (d) D. MacGowan, J. Chem. Phys. 81, 3224 (1984).

24. M. Ross and F. H. Ree, J. Chem. Phys. 73, 6146 (1980).

25. F. H. Ree, J. Chem. Phys. 76, 6287 (1982).

26. A. C. Mitchell and W. J. Nellis, J. Chem. Phys. 76, 6273 (1982).

27. J. M. Walsh and M. H. Rice, J. Chem. Phys. 26, 815 (1957).

28. W. Keesom, Z. Phys. 22, 129 (1921).

29. (a) W. J. Nellis and A. C. Mitchell, J. Chem. Phys. 73, 6137 (1980); (b) W. J. Nellis, N. C. Holmes, A. C. Mitchell, and M. van Thiel, Phys. Rev. Letters, 53, 1661 (1984); (c) H. B. Radousky and W. Nellis have recently found that nitrogen "shock-cools," when it it is doubly shocked from the first shock pressures near or within the range where the softening takes place. The corresponding shock temperatures are still relatively high (> 7000 K) for explosive-related problems. This work will be published.

30. S. P. Marsh, LANL Shock Hugoniot Data (University of California, Berkeley, 1980), p. 113.

31. V. N. Zubarev and G. S. Telegin, Sov. Phys. Doklady 7, 34 (1962).

32. (a) R. Grover and F. H. Ree, in High Pressure in Research and Industry, Vol. 1, C. M. Backman, T. Johannison, and L. Tegner, Eds. (Arkitektokpia, Sweden, 1982), p. 217; (b) A. K. McMahan and R. LeSar, Phys. Rev. Lett. 54, 1929 (1985); (c) M. Ross, to be published.

33. (a) N. C. Holmes, W. J. Nellis, W. B. Graham, and G. E. Walrafen, Phys. Rev. Lett. 55, 2433 (1985); (b) W. Nellis, private communication.

34. S. D. Hamann, in Modern Aspects of Electrochemistry, B. E. Conway and J. O'M. Bockris, Eds. (Plenum, New York, 1974), No. 9, p. 131.

35. T. M. Reed and K. E. Gubbins, Applied Statistical Mechanics (McGraw Hill, New York, 1973), p. 32.

36. G. A. Mansoori and E. B. Canfield, J. Chem. Phys. 51, 4958 (1968).

37. J. Rasaiah and G. Stell, Mol. Phys. 18, 249 (1970).

38. M. Ross, J. Chem. Phys. 71, 1567 (1979).

39. H. S. Kang, C. S. Lee, T. Ree, and F. H. Ree, J. Chem. Phys. 82, 414 (1985).

40. D. A. Young and F. J. Rogers, J. Chem. Phys. 81, 2789 (1984).

41. H. B. Levine, "Final Report on the Method of Univariant Descent for Solving Problems in Heterogeneous Chemical Equilibria," (Jaycor, Del Mar, 1982). This work was undertaken under a contract with the Lawrence Livermore National Laboratory.

42. M. Finger, E. Lee, F. H. Helm, B. Hayes, H. Hornig, R. McGuire, and M. Kahara, in Proceedings of the Sixth Symposium (International) on Detonation, D. J. Edwards, Ed., ACR-221 (Office of Naval Research, Department of the Navy, 1976), p. 710.

43. C. L. Mader, Numerical Modeling of Detonations, (University of California, Berkeley, 1979).

44. R. G. McQueen, S. P. Marsh, J. W. Taylor, J. N. Fritz, and W. J. Carter, High Velocity Impact Phenomena, R. Kinslow, Ed. (Academic, New York, 1970), p. 293.

45. (a) J. H. Kineke, Jr. and C. E. West, in Proceedings of the Fifth Symposium (International) on Detonation, ACR-184 (Office of Naval Research, Department of the Navy, 1970), p. 533; (b) J. H. Kineke, Jr., "Shocked States of Seven Overdriven Explosives," Ballistic Research Laboratories, Rept. DEA-G-1060MTG (1970).

46. (a) E. L. Lee, M. van Thiel, L. G. Green, and A. Mitchell, in Shock Waves in Condensed Matter - 1983, J. R. Asay, R. A. Graham, and G. K. Straub, Eds., (Elsevier Science, 1984), p. 617; (b) L. Green, E. L. Lee, A. Mitchell, and C. Tarver, in Ref. 5.

47. (a) E. L. Lee, H. C. Hornig, and J. W. Kury, "Adiabatic Expansion of High Explosive Detonation Products," Lawrence Livermore National Laboratory, Livermore, CA, UCRL-50422 (1968); (b) W. C. Davis and J. B. Ramsay, in Ref. 42, p. 531.

48. H. C. Hornig, E. L. Lee, M. Finger, and J. E. Kurrle, in Ref. 45 (a), p. 503.

49. (a) V. M. Prokhorov and D. S. Tsiklis, Russian J. Phys. Chem. 44, 1173 (1980); (b) D. S. Tsiklis and V. Ya. Maslennikova, Pokl. Akad. Nauk. SSSR 161, 645 (1965).

50. K. Tödheide and E. U. Franck, Zeitschrift für Physikalische Chemie Naue Folge 37, 387 (1963).

51. A. Kreglevskii, Bull. Acad. Polon. Sci. Cl. III 5, 667 (1957).

52. G. Scoles, in Ann. Rev. Phys. Chem., Vol. 31 (Annual Reviews, 1980), p. 81.

53. J. W. Kury, H. C. Hornig, E. L. Lee, J. L. McDonnel, D. L. Ornellas, M. Finger, F. M. Strange, and M. L. Wilkins, in Proceedings of the Fourth Symposium (International) on Detonation, ACR-126 (Office of Naval Research, Dept. of the Navy, 1965), p. 3.

54. R. D. Cowan and W. Fickett, J. Chem. Phys. 24, 932 (1956).

55. (a) S. J. Jackobs, in Proceedings of the Twelfth Symposium on Combustion, (The Combustion Institute, Pittsburgh, 1969), p. 501; (b) M. Cowperthwaite and W. H. Zwisler in Ref. 42, p. 162.

56. D. J. Steinberg, in Ref. 5.

57. See footnotes in Table IV for experimental references.

58. R. Cheret, C. R. Acad. Sc. Paris 274, 1347 (1972).

59. M. Costantino and F. H. Ree, unpublished work.

60. D. Schiferl, R. L. Mills, L. C. Schmidt, C. Vanderborgh, E. F. Skelton, W. T. Elam, A. W. Webb, L. C. Ming, J. Baloogh, and M. H. Manghnani, Physica B (to appear).

61. T. W. Melnyk and B. L. Sawford, Mol. Phys. 29, 891 (1975).

62. (a) J. L. Lebowitz and J. S. Rowlinson, J. Chem. Phys. 41, 133 (1964); (b) J. L. Lebowitz and D. Zomick, J. Chem. Phys. 54, 3335 (1971).

63. B. J. Alder, J. Chem. Phys. 40, 2724 (1964).

64. D. J. Stevenson, in Ref. 12a, Vol. III, p. 337.

0667M/0553M

Figure captions

Fig. 1. Comparison of experimental and theoretical Hugoniots of N_2, H_2O, and CO_2. The experimental data are from the Lawrence Livermore National Laboratory (LLNL) [Ref. 26 (H_2O) and Ref. 29 (N_2)], the Los Alamos National Laboratory (LANL) [Ref. 27 (H_2O) and Ref. 30 (N_2)], and Zubarev and Telegin (Ref. 31). The solid lines are based on of Ref. 24 (N_2 and CO_2) and Ref. 2b (H_2O). The dotted line is obtained using the exp-6 parameters of the WCA4 theory (Ref. 3b) and the JCZ3 theory (Ref. 42), without the electrostatic dipole contribution. Note that the initial density of solid CO_2 in Ref. 31 is in error. This has been corrected here and also in Ref. 24.

Fig. 2. Comparison of experimental (Refs. 45 and 46) and theoretical shock velocity vs shock pressure for PBX-9404: (a) the CHEQ 2-phase calculation assumes a homogeneous phase of fluid mixture and a solid phase of carbon that can be either graphitic or diamond-like (see Sec. 3); (b) the CHEQ 3-phase calculation considers two fluid phases (N_2-rich and N_2-poor fluids) and a solid carbon phase (see Sec. 5).

Fig. 3. Solubility isotherms vs molar concentrations at different temperatures for three binary systems: (a) N_2-H_2O, (b) CO_2-H_2O, and (c) N_2-CO_2 systems. These are computed using unlike-pair exp-6 parameters: $r^*_{N_2-H_2O} = 3.575$ Å, $r^*_{CO_2-H_2O} = 3.615$ Å, and $r^*_{N_2-CO_2} = 4.13$ Å. Other parameters employed here are given in Table I and Eqs. (7) to (9). Dashed or broken portions of the isotherms indicate that the free energy difference is too small for the CHEQ code to give reliable results.

Fig. 4. Dependence of solubility isotherms on unlike-pair exp-6 parameters. The solid and dotted lines are based on the use of $r^*_{N_2-H_2O} = 3.575$ Å [Eq. (10)] and 3.682 Å [Eq. (11)], respectively. The dashed or broken sections of the isotherms represent computationally uncertain portions.

Fig. 5. Critical solubility lines of the three binary mixtures considered in Figs. 3 and 4. The solid lines are based on the exp-6 parameters of Fig. 3, while the dotted line is based on $r^*_{N_2-H_2O}$ = 3.682 Å, the value used for the dotted lines in Fig. 4. The low-T portion of the N_2-H_2O critical line has a larger uncertainty for reasons explained in the text. Theoretical Hugoniot paths of PBX-9404 and PETN are shown for comparison. Solid circles represent the CJ points of these explosives.

Fig. 6. Phase diagram of a ternary (N_2-CO_2-H_2O) mixture at T = 0.35 eV and P = 33 GPa. The shaded region is the mixed fluid phase region based on the exp-6 parameters of Eq. (10). The area under the dotted line represents the mixed phase region if Eq. (11) is used for the exp-6 parameters.

Fig. 7. The Chapman-Jouguet (CJ) expansion adiabats of PBX-9404 (ρ_0 = 1.84 g/cm^3) predicted by the present theory (CHEQ), the BKW EOS, the JCZ3 EOS, and the JWL EOS (Ref. 54). For comparison, the JWL EOS can be considered "experimental" data. See the text.

Fig. 8. The Grüneisen γ along the CJ adiabats (both compression and expansion) of PBX-9404 (ρ_0 = 1.84 g/cm^3) computed from various models in Fig. 7. Note that the JWL EOS assumes a constant value for γ. The dotted and broken parts of the γ (CHEQ) represent computationally uncertain portions.

Fig. 9. Theoretical Hugoniots of RDX at various initial densities (ρ_0). Wiggly structures in some of the Hugoniots occur within the supercritical fluid phase separation involving the N_2-rich and N_2-poor fluid phases. Note that there are two roots (i.e., double minima) for the Chapman-Jouguet (CJ) point for ρ_0 = 1.55 g/cm^3 and 1.60 g/cm^3.

Fig. 10. Comparison of the experimental Chapman-Jouguet data (Refs. 56 and 57) of RDX and the theoretical results obtained from the absolute minima (solid circles) in Fig. 9: (a) D_{CJ} vs ρ_o; (b) P_{CJ} vs ρ_o. The dotted lines indicate the supercritical fluid phase separation boundary where theoretical uncertainties are large. See the text.

Table I. Parameters of exponential-6 potentials [Eqs. (2) and (6)] for chemical species considered in calculations of explosives.[a]

Species	ϵ/k (K)	r^* (Å)	α	λ (K)
H_2	36.4	3.43	11.1	0
N_2	101.9	4.09	13	0
O_2	125.0	3.84	13	0
CO	108.3	4.12	13	0
CO_2	245.6	4.17	13	0
CH_4	154.1	4.22	13	0
NO	112.9	3.97	13	0
H_2O	356.0	3.06	13	996.8
NH_3	474.0	3.44	13	441.0
C_2H_2	249.4	4.50	13	0
C_2H_6	246.8	4.86	13	0
C_3H_8	298.9	5.43	13	0
CH_3OH	414.6	4.92	13	0
N_2O	250.1	4.26	13	0
NO_2	348.4	4.27	13	0
HCN	369.0	5.54	13	0
HCl	262.3	4.14	13	0
Cl_2	336.9	4.61	13	0
PH_3	262.4	4.49	13	0

a Parameters for the first nine species are from Ref. 2a. See references quoted therein for original experimental data. Parameters for the rest of the chemical species are derived here using the corresponding state scaling relation (Ref. 24).

Table II. Dependence of the Chapman-Jouguet velocity (D_{CJ}) of PBX 9404 on various physical parameters. Initial density (ρ_0) = 1.84 g/cm^3.[a]

Calculation	Type	D_{CJ} (km/s)
(A)	Solid C + single gas phase (11 species)	9.30
(B)	(A) + C_2H_2, C_2H_6, C_3H_8, CH_3OH	9.35
(C)	(A) + N_2O, NO_2, HCN	9.30
(D)	(A) + HCl, Cl_2, PH_3, P_4O_{10} (solid)	9.25
(E)	No solid carbon (single gas phase)	9.82
(F)	(A) with ΔH_f° (diamond) = 15 kcal/mole	9.53
(G)	(A) with $k_{H_2O-N_2}$ = 1.03 and $k_{H_2O-CO_2}$ = 0.965	9.35
	Experiment	8.80

a These calculations assume all gas species are in a single phase. Calculation (A) corresponds to the calculation described in Sec. 3.

Table III. Comparison of the Chapman-Jouguet data of PBX-9404 between the experimental data and the CHEQ calculations (ρ_0 = 1.84 g/cm^3).

	D_{CJ} (km/s)	P (GPa)	ρ (g/cm^3)	T (K)
Experiment	8.80[a]	37[a]	2.48	--
	8.78 ± 0.01[b]	35.6 ± 0.4[b]	2.46	--
CHEQ-3 phase[c]	8.81	33.2	2.40	4089
CHEQ-2 phase[c]	9.35	35.0	2.35	3809
CHEQ-2 phase[d]	9.30	34.7	2.35	3847

[a] Ref. 47a.

[b] Ref. 47b (ρ_0= 1.846 g/cm^3).

[c] These results are based on Eq. (11), i.e., $r^*_{H_2O-N_2}$ = 3.682 Å and $r^*_{H_2O-CO_2}$ = 3.488 Å.

[d] These results are based on Eq. (10), i.e., $r^*_{H_2O-N_2}$ = 3.575 Å and $r^*_{H_2O-CO_2}$ = 3.615 Å.

Table IV. Comparison of experimental and theoretical (CHEQ) Chapman-Jouguet shock velocities (D_{CJ}) and pressures (P_{CJ}) at different initial densities of RDX. The theoretical results are based on the PBX-9404 EOS data computed by the CHEQ code and the experimental heat of formation of RDX. For a more complete compilation of the experimental D_{CJ} data, see Steinberg's paper.[56]

Initial Density (g/cm^3)	D_{CJ} (km/s)		P_{CJ} (GPa)		References
	Experiment	This work	Experiment	This work	
0.53	4.06	4.14	--	2.79	1
0.56	4.05	4.25	3.16	3.06	2
0.61	4.39	4.45	--	3.55	1
0.70	4.78, 4.65	4.81	4.72	4.57	1, 2
0.90	5.61, 5.75	5.65	--	7.64	3
0.95	5.80	5.87	9.46	8.54	2
1.00	6.04	6.08	--	9.59	1
1.05	6.19	6.30	--	10.67	3
1.07	6.26	6.38	11.6	11.15	2
1.10	6.18	6.51	12.0	11.94	2
1.20	6.75	6.89	15.2	15.19	3, 4
1.29	7.00	7.15	16.4	17.46	2
1.40	7.44	7.49	21.3	19.97	4
	7.45, 7.42				3, 6
1.46	7.60	7.70	20.8	21.59	2
1.501	7.69	7.85	--	22.63	7
1.59	8.10, 8.14	8.17	28.7	29.66	4, 5
1.60	8.13, 8.10	8.18	26.0	29.85	2, 3
1.72	8.46, 8.50	8.44	30.8	30.97	2, 5
	8.51				3
1.77	8.64	8.61	33.8	31.60	8

1. L. N. Stesik and N. S. Shvedova, Zhurnal Prikladnoi Mekhaniki i Technicheskoi Fisiki, No. 4, 124 (1964).
2. N. M. Kuznetsov and K. K. Shvedov, Combustion, Explosion, and Shock Waves 2, 52 (1966).
3. Los Alamos National Laboratory, GMX-8 unpublished data, July 1956.
4. A. N. Dremin and P. F. Pokhil, Acad. Sci. USSR, Proc. Phys. Chem. 128, 839 (1959).
5. A. N. Dremin and K. K. Shvedov, Zhurnal Prikladnoi Mekhaniki i Technicheskoi Fisiki, No. 2, 154 (1964).
6. Los Alamos National Laboratory, GMX-8, Progress Report, July 1957.
7. Los Alamos Explosives Performance Data, C. L. Mader, J. N. Johnson, and S. L. Crane, Eds., (Univ. of Calif., Berkeley, 1982), p. 348.
8. W. E. Deal, J. Chem. Phys. 27, 124 (1964).

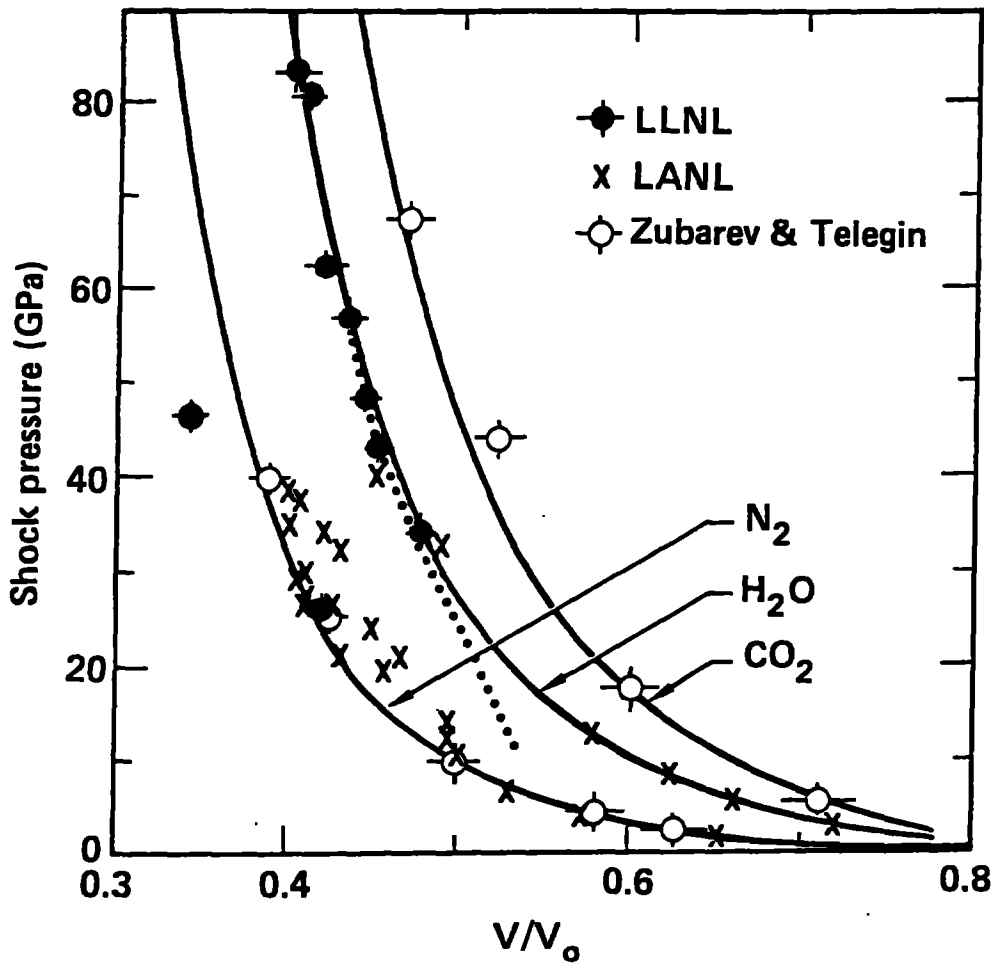
LLNL
LANL
Zubarev & Telegin
N_2
H_2O
CO_2
Shock pressure (GPa)
0
20
40
60
80
0.3
0.4
0.6
0.8
V/V_o

Fig. 1

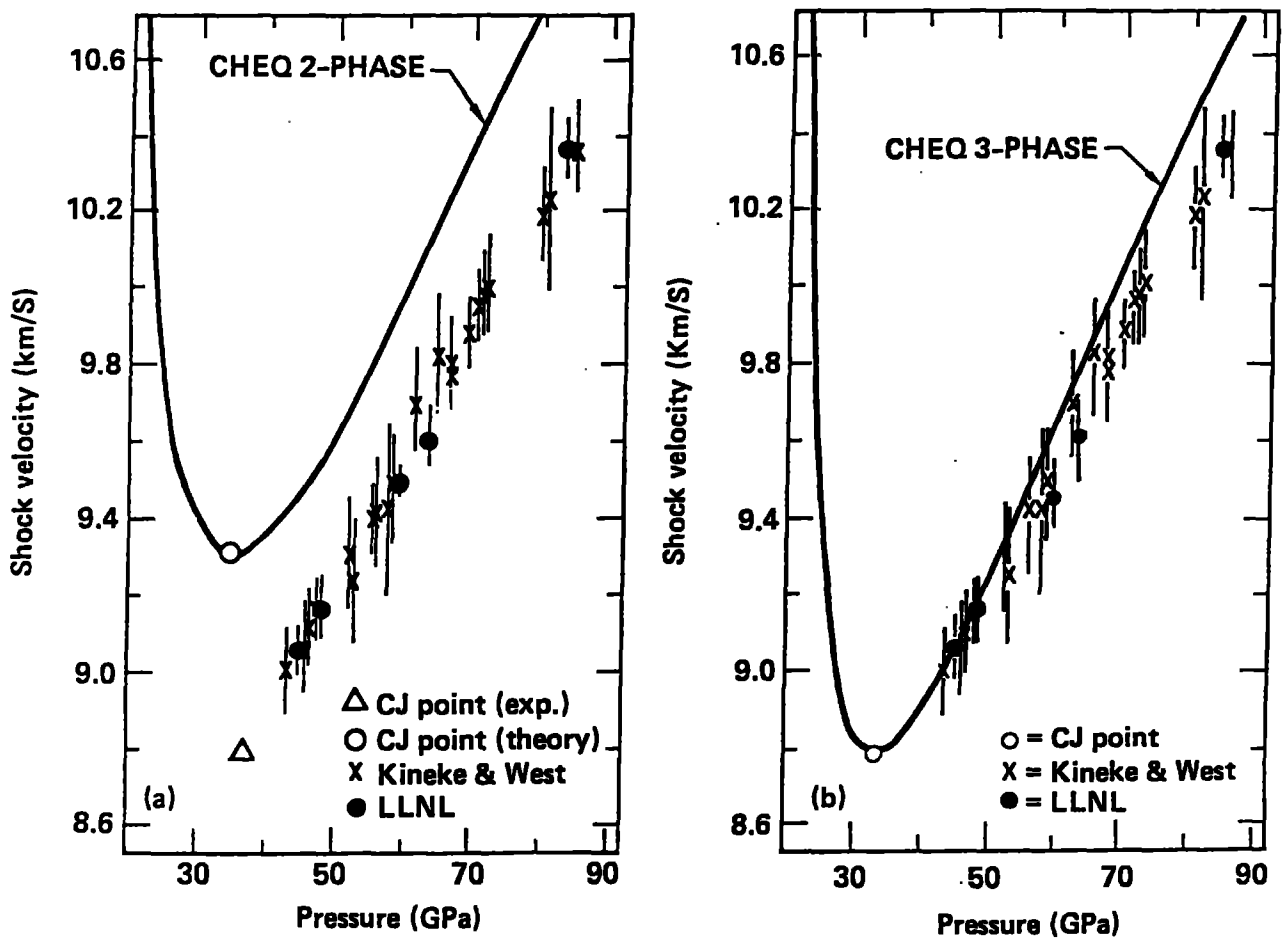
CHEQ 2-PHASE
CHEQ 3-PHASE
Shock velocity (km/S)
Shock velocity (Km/S)
Pressure (GPa)
10.6
10.2
9.8
9.4
9.0
8.6
30
50
70
90
△ CJ point (exp.)
○ CJ point (theory)
X Kineke & West
● LLNL
(a)
○ = CJ point
X = Kineke & West
● = LLNL
(b)

Fig. 2

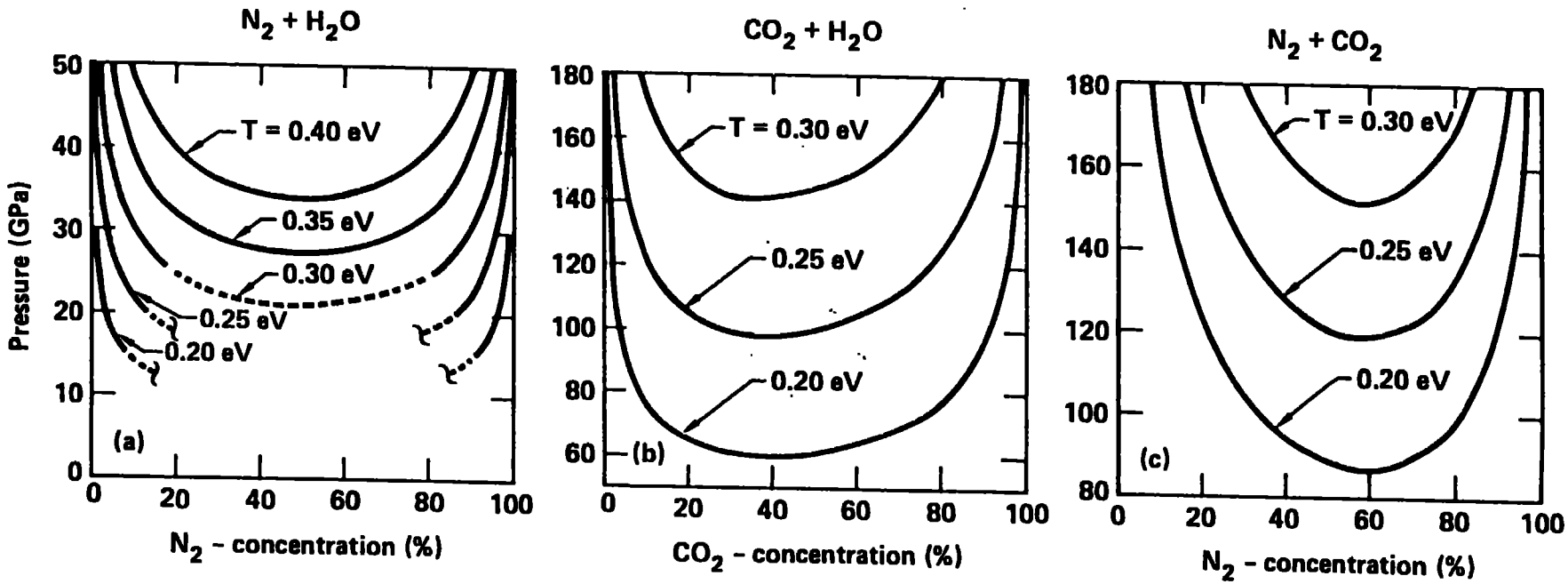
$N_2 + H_2O$
$CO_2 + H_2O$
$N_2 + CO_2$
Pressure (GPa)
T = 0.40 eV
0.35 eV
0.30 eV
0.25 eV
0.20 eV
T = 0.30 eV
0.25 eV
0.20 eV
T = 0.30 eV
0.25 eV
0.20 eV
(a)
(b)
(c)
N_2 - concentration (%)
CO_2 - concentration (%)
N_2 - concentration (%)

Fig. 3

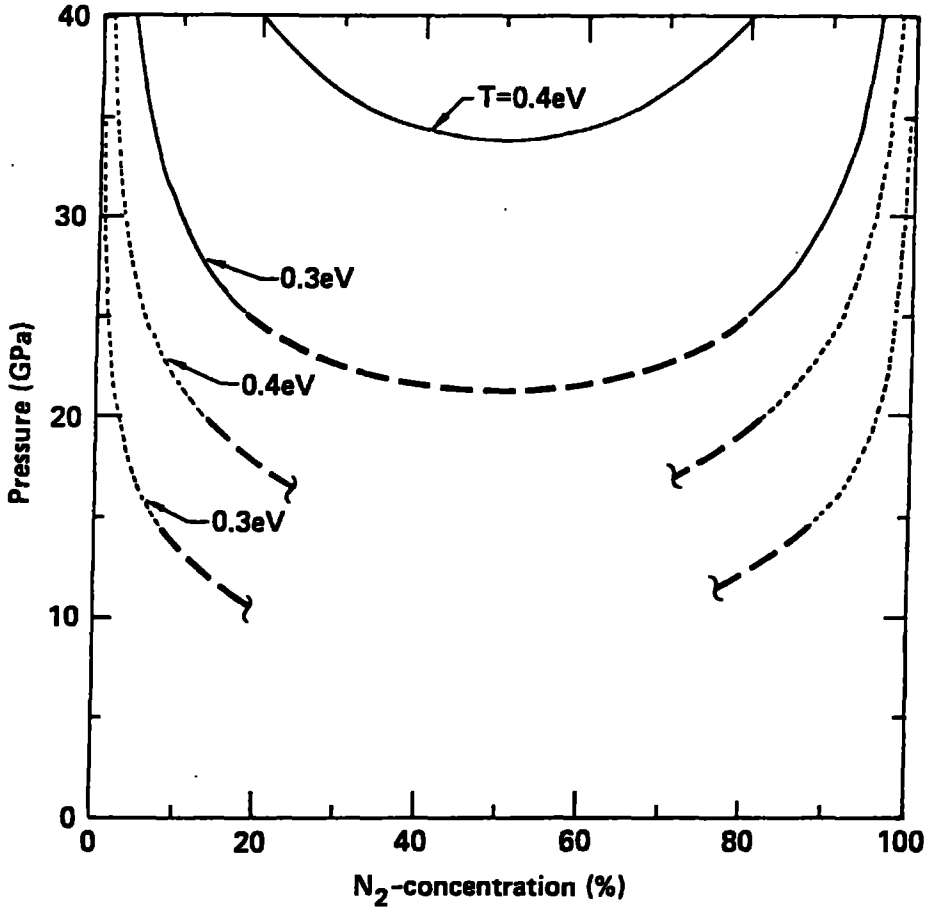
40
30
20
10
0
Pressure (GPa)
T=0.4eV
0.3eV
0.4eV
0.3eV
0
20
40
60
80
100
N2-concentration (%)

Fig. 4

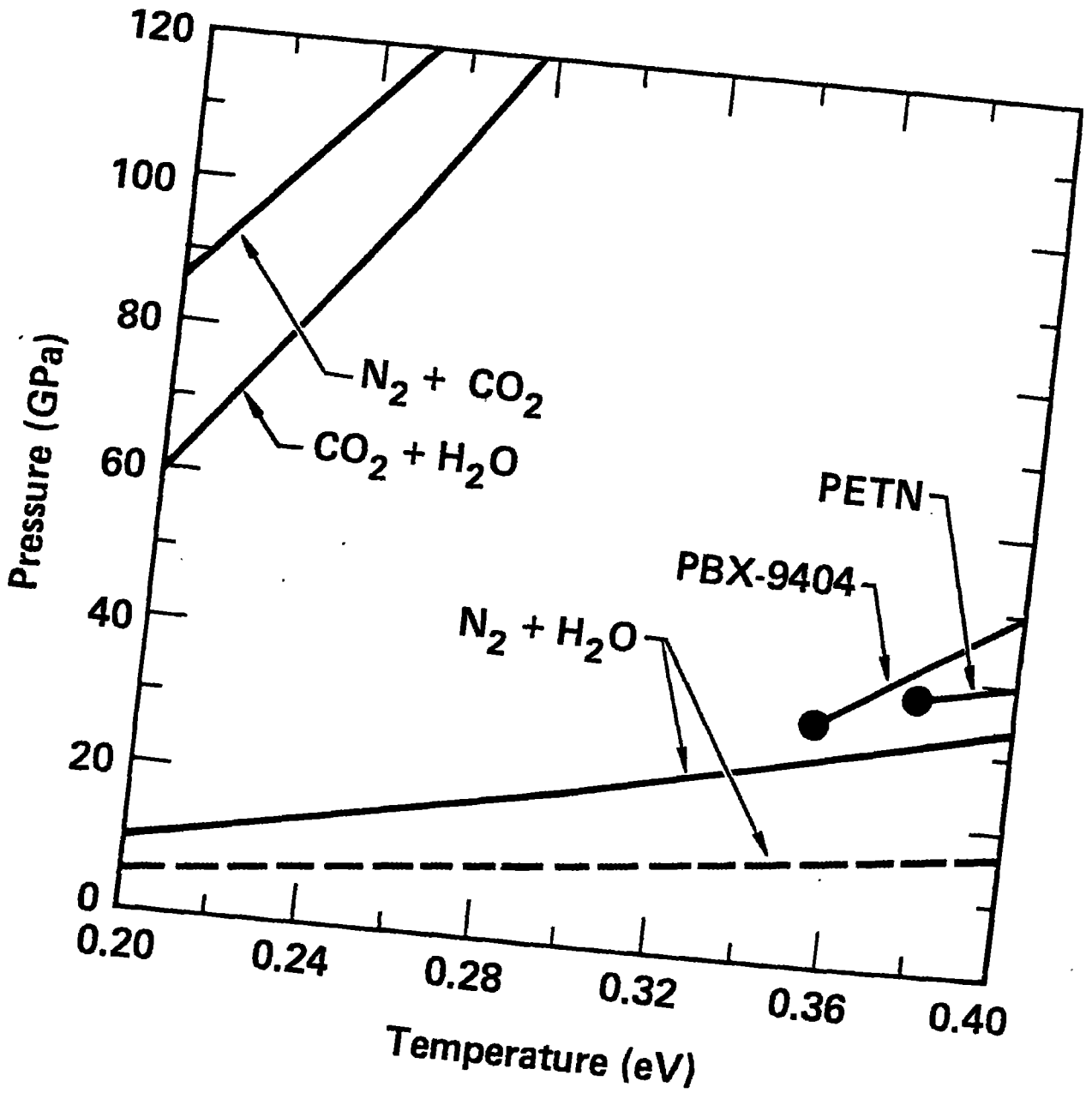
120
100
80
60
40
20
0
Pressure (GPa)
$N_2 + CO_2$
$CO_2 + H_2O$
PETN
PBX-9404
$N_2 + H_2O$
0.20
0.24
0.28
0.32
0.36
0.40
Temperature (eV)

Fig. 5

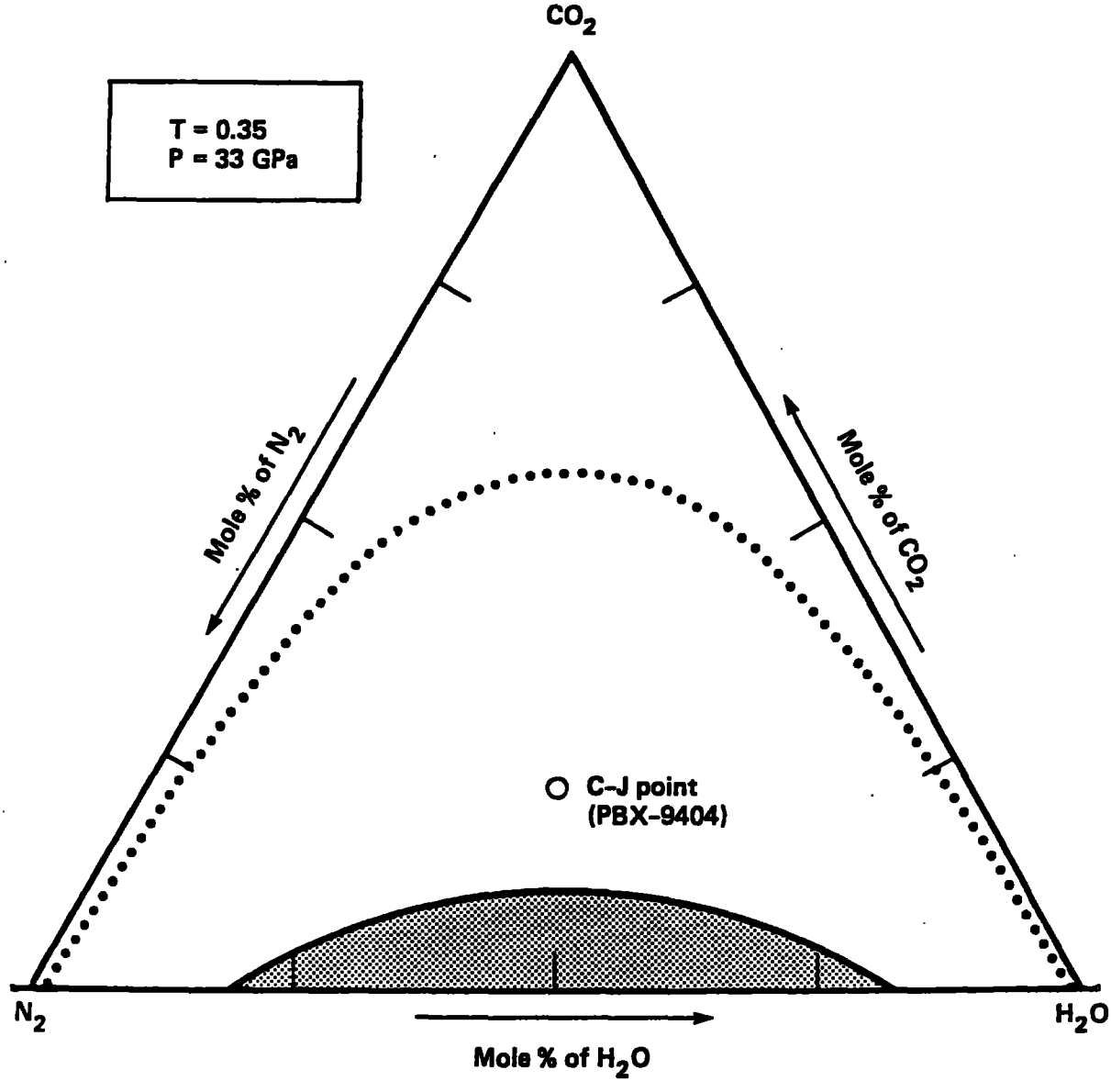
CO_2
T = 0.35
P = 33 GPa
Mole % of N_2
Mole % of CO_2
C-J point
(PBX-9404)
N_2
H_2O
Mole % of H_2O

Fig. 6

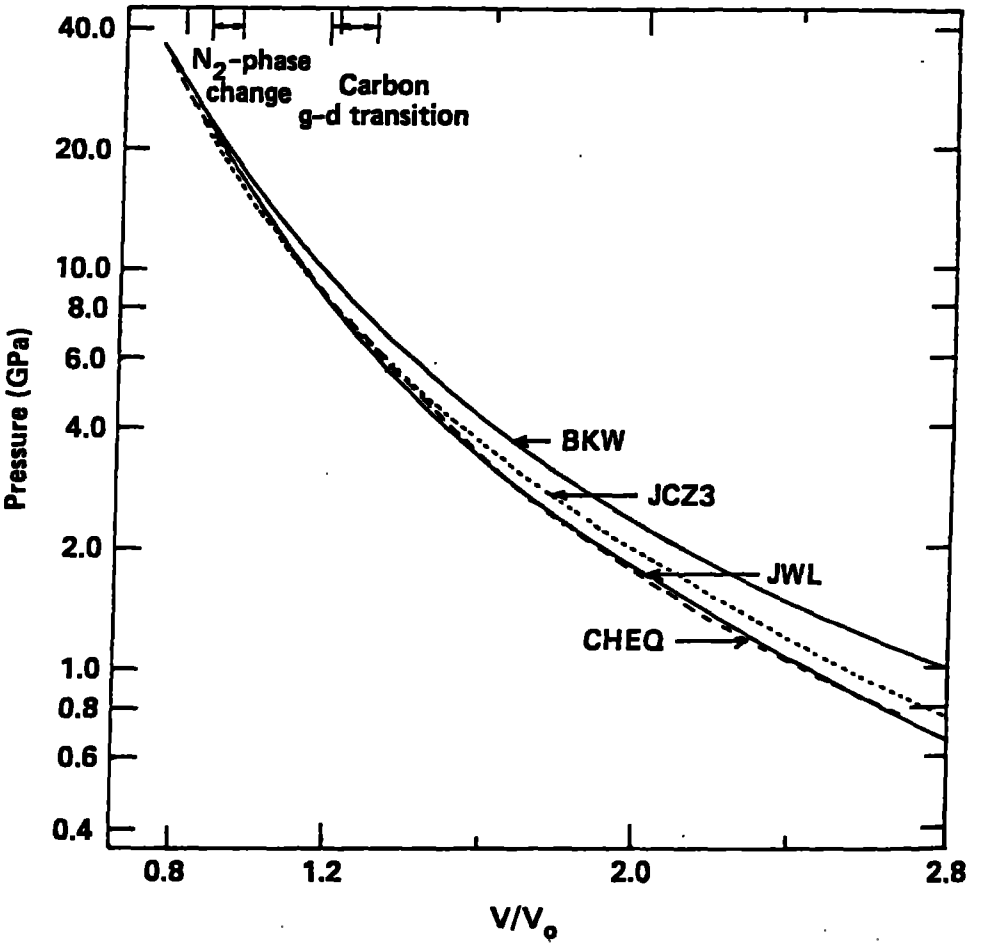
40.0
20.0
10.0
8.0
6.0
4.0
2.0
1.0
0.8
0.6
0.4
Pressure (GPa)
N_2-phase change
Carbon g-d transition
BKW
JCZ3
JWL
CHEQ
0.8
1.2
2.0
2.8
V/V_o

Fig. 7

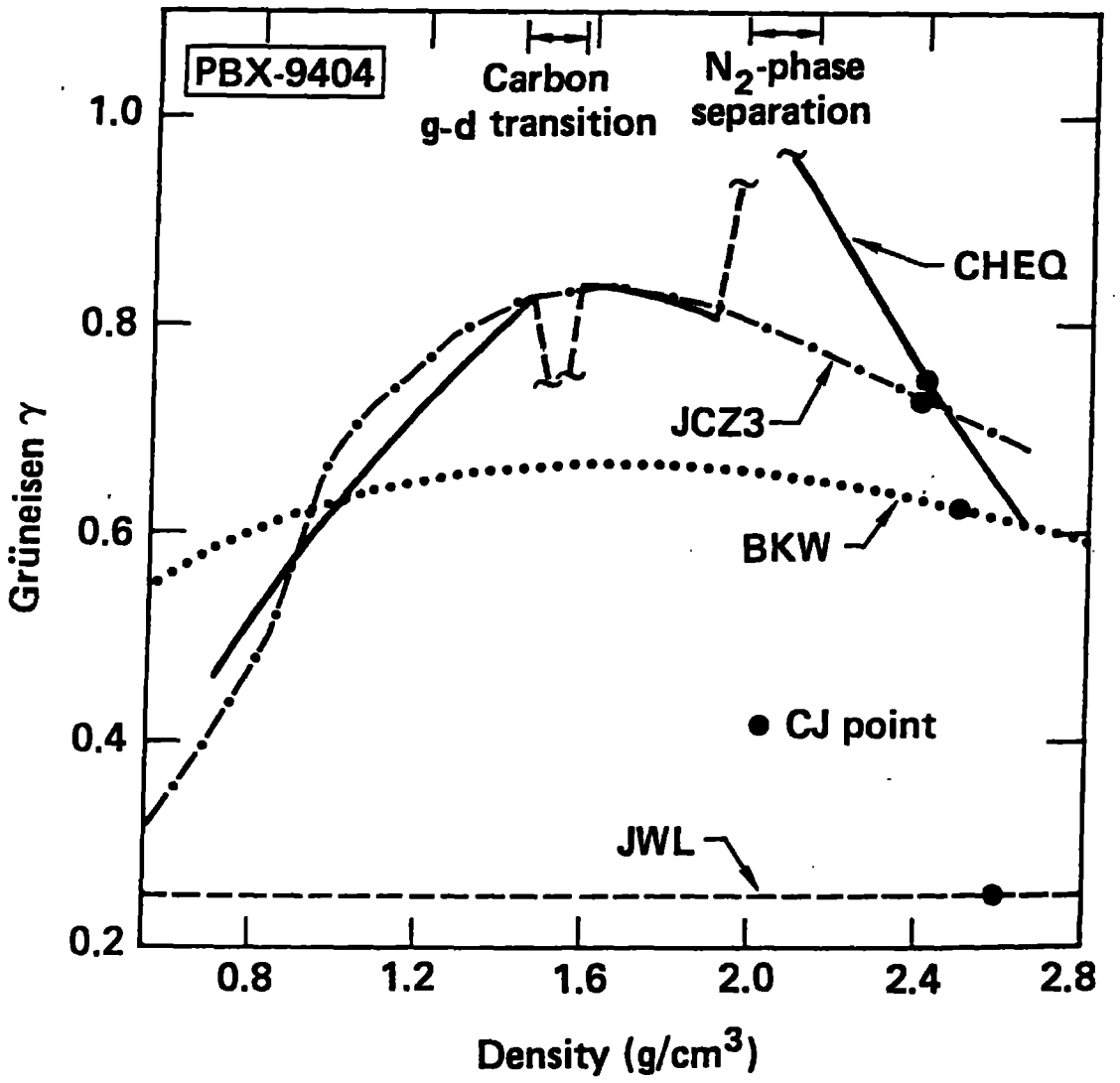
PBX-9404
Carbon
g-d transition
N_2-phase
separation
CHEQ
JCZ3
BKW
CJ point
JWL
Grüneisen γ
1.0
0.8
0.6
0.4
0.2
0.8
1.2
1.6
2.0
2.4
2.8
Density (g/cm^3)

Fig. 8

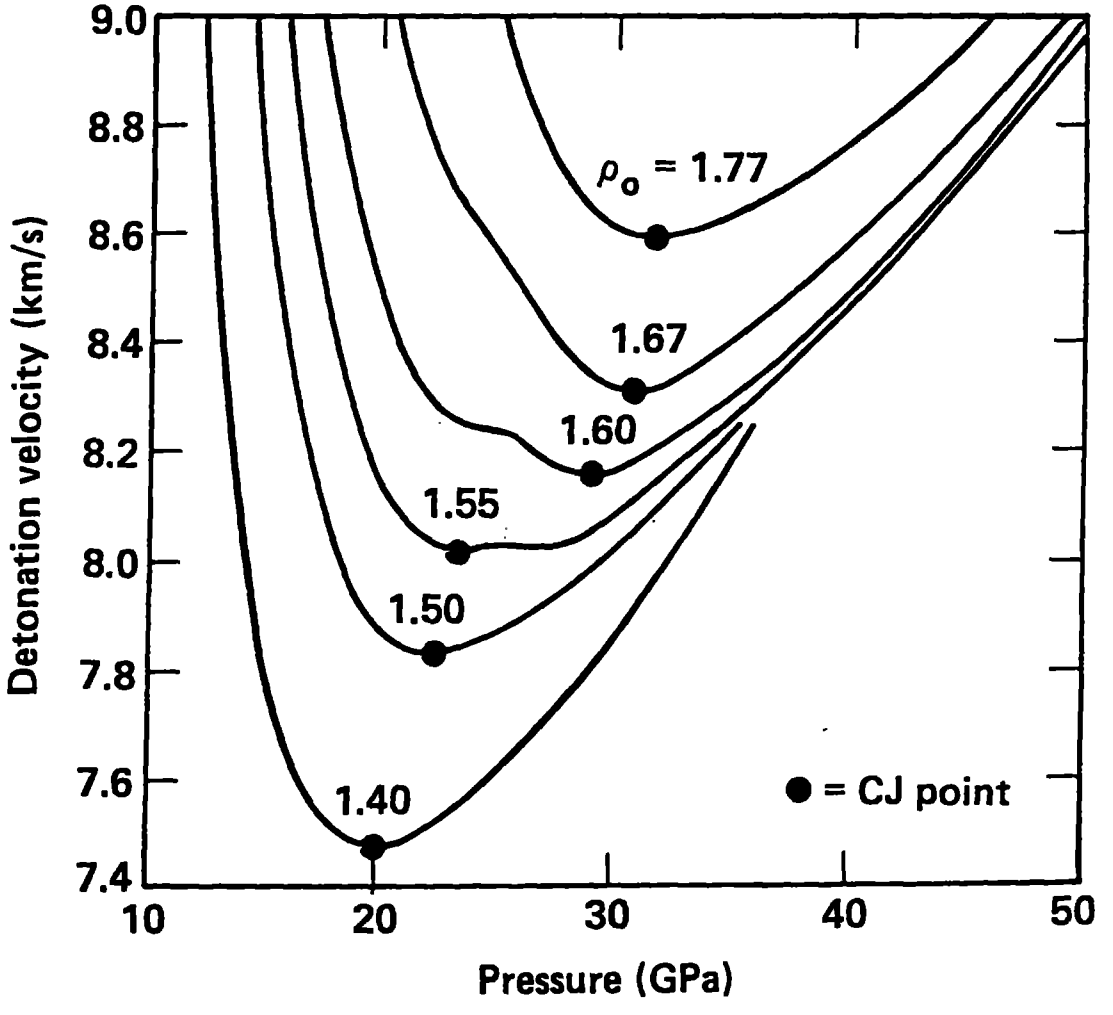
9.0
8.8
8.6
8.4
8.2
8.0
7.8
7.6
7.4
Detonation velocity (km/s)
10
20
30
40
50
Pressure (GPa)
ρ_o = 1.77
1.67
1.60
1.55
1.50
1.40
● = CJ point

Fig. 9

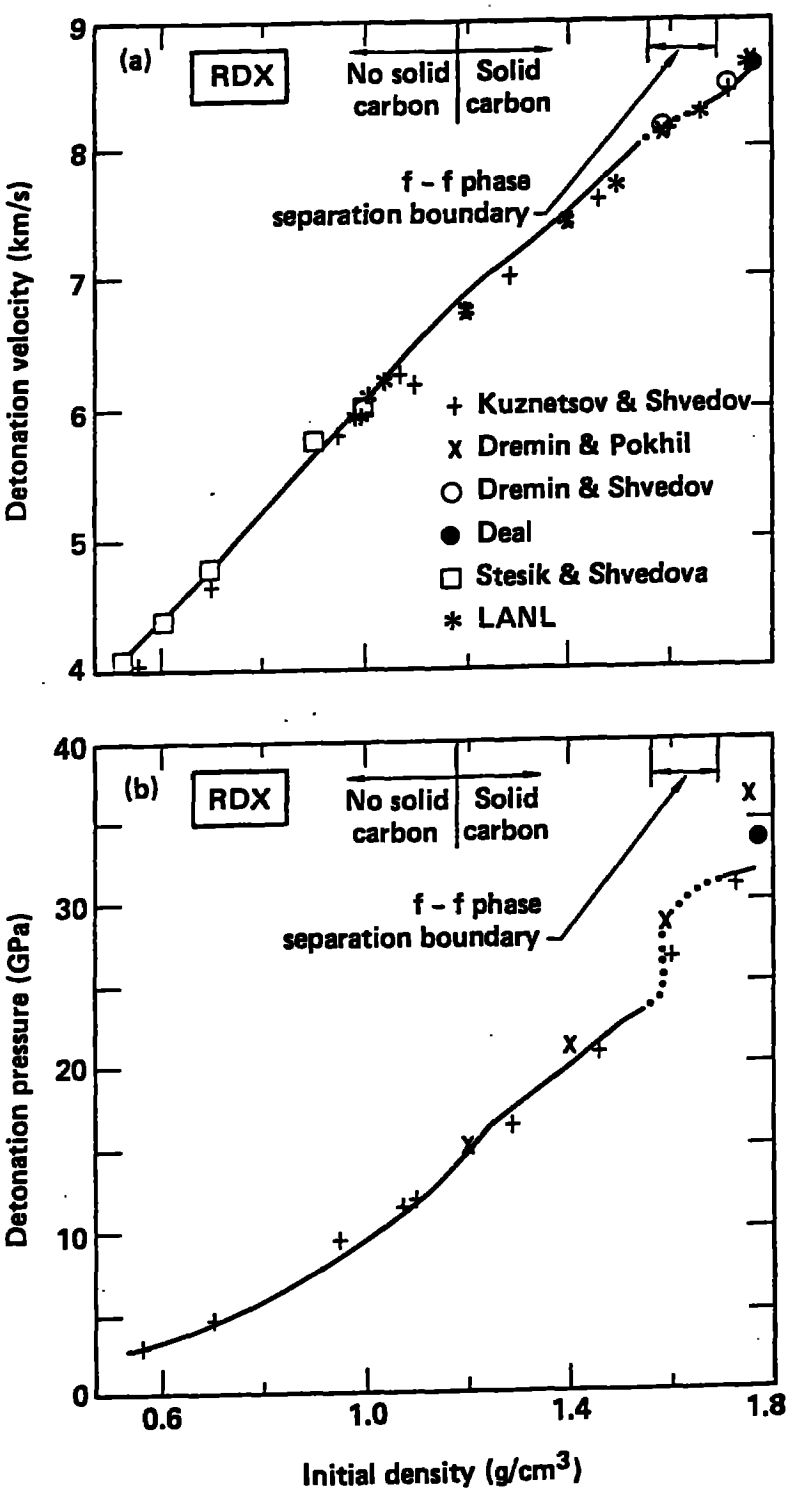
(a)
RDX
No solid carbon
Solid carbon
f - f phase separation boundary
+ Kuznetsov & Shvedov
x Dremin & Pokhil
○ Dremin & Shvedov
● Deal
□ Stesik & Shvedova
* LANL
Detonation velocity (km/s)
9
8
7
6
5
4
(b)
RDX
No solid carbon
Solid carbon
f - f phase separation boundary
Detonation pressure (GPa)
40
30
20
10
0
0.6
1.0
1.4
1.8
Initial density (g/cm3)

Fig. 10